Figure S1. Pictures of the three extraction fronts of feldspars from LLANSÀ S.A. and the name of the sample obtained from each front.

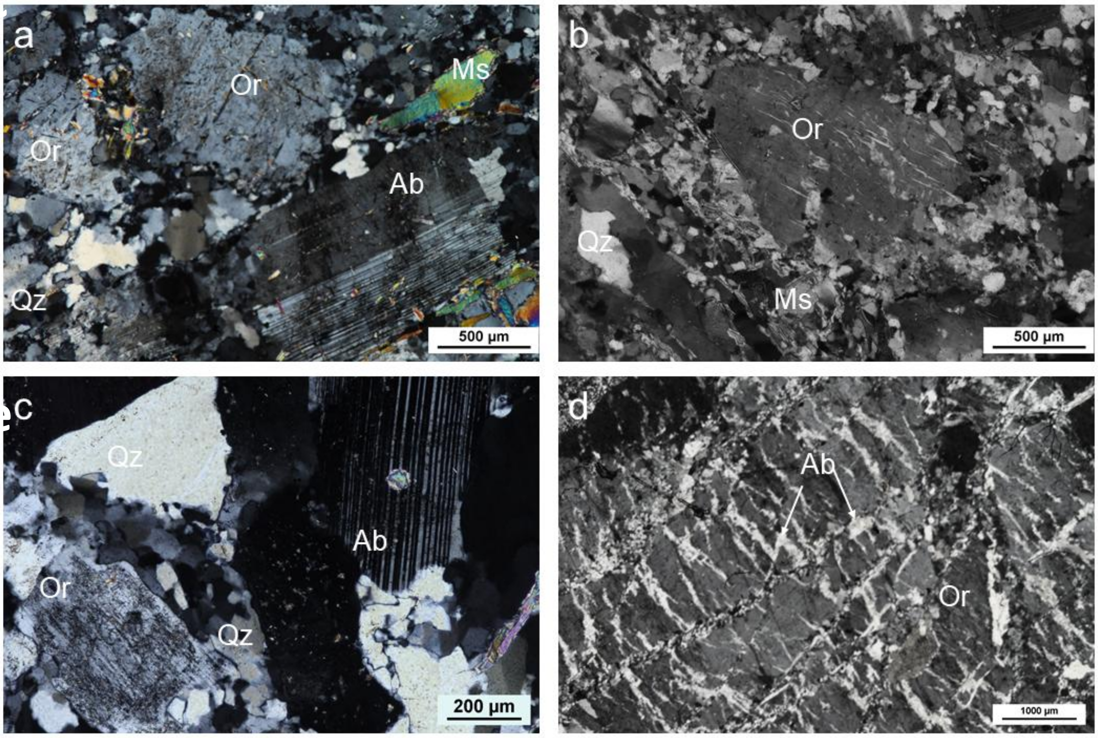

Figure S2. Photomicrographs (under crossed polars) corresponding to three exploration levels of the pegmatitic feldspars from Llançà. a) granular texture formed by a large euhedral albite crystal showing polysynthetic twinning and an hemihedral orthoclase crystal, surrounded by small anhedral quartz and muscovite crystals. b) The central part shows an hemihedral orthoclase crystal with microperthite texture surrounded by quartz. c) Euhedral albite (polysinthetic twining) and orthoclase being altered to kaolinite and sericite accompanied with several sizes of quartz grains. d) Perthitic texture shows fine lamellar albite crystals forming a braided pattern in an orthoclase host. Or, Orthoclase; Ab, albite; Ms, muscovite.

Table S1. Bulk chemical composition of the studied feldspars, expressed as wt% oxides determined by XRF. Oxide ratios (K_2O/Na_2O and SiO_2/Al_2O_3) and Loss on ignition (LOI) are also reported.

Sample name	Texture	Main polymorph	SiO_2	Al_2O_3	Na_2O	K_2O	CaO	K_2O/ Na_2O	SiO_2/ Al_2O_3	MgO	Fe_2O_3	TiO_2	P_2O_5	LOI
IK1	Perthitic	Mc	64.97	18.81	2.95	12.78	0.32	4.3	3.4	0.03	0.06	0	0.07	–
IK2	Perthitic	Mc	65.84	18.76	3.31	11.86	0.1	3.6	3.5	0.01	0.1	0	0.01	0.19
LNaK1	Perthitic	Or/Mc	75.18	14.85	3.67	3.78	0.79	1.0	5.1	0.17	0.62	0.08	0.29	0.83
LNaK2	Perthitic	Or/Mc	73.23	15.30	5.13	4.83	0.65	0.9	4.8	0.06	0.11	0.01	0.31	0.38
LNa1	Anti-perhtitic	Ab	75.67	14.17	5.91	2.27	0.73	0.4	5.3	0.07	0.14	0.02	0.30	0.35
LNa2	Anti-perhtitic	Ab	75.71	14.46	6.84	1.38	0.75	0.2	5.2	0.07	0.15	0.02	0.30	0.44

Table S2. Trace elements concentration (in ppm) measured using XRF for the feldspar powders. Values reported as <ld indicate concentrations below the detection limit. Rb and Sr values are highlighted in red due to their direct mention in the main text.

ppm	IK1	IK2	LNaK1	LNaK2	LNa1	LNa2
As	3.7	< ld	< ld	1.96	< ld	< ld
Ba	60.1	59.5	141.7	314.1	147.8	116.3
Ce	< ld	< ld	6.7	< ld	< ld	< ld
Co	< ld	< ld	< ld	69.6	< ld	< ld
Cr	< ld	< ld	< ld	< ld	< ld	< ld
Cu	5	1.5	1.2	< ld	0.3	0.2
Ga	11.1	28.9	24.5	16.2	20.7	20.0
La	< ld	1.8	< ld	< ld	< ld	< ld
Mo	0.2	< ld	< ld	< ld	< ld	< ld
Nb	8.9	9.1	16.7	19.3	13.9	13.1
Nd	< ld	< ld	< ld	< ld	< ld	< ld
Ni	1.7	< ld	< ld	< ld	< ld	< ld
Pb	187.5	9.2	34.3	8.2	14.0	14.6
Rb	**839.2**	**607.2**	**181.9**	**159.3**	**102.4**	**64.5**
Sc	< ld	< ld	2.4	< ld	< ld	< ld
Sn	5.2	< ld	13.1	5.0	5.7	4.6
Sr	**25.2**	**26.6**	**54.9**	**132.9**	**92.6**	**78.8**
Th	2.6	3.3	4.1	2.7	3.2	2.9
V	4.8	4.3	8.8	5.7	6.6	6.1
W	< ld	11.4	1.4	575.1	< ld	< ld
Y	24	17.8	14.2	7.4	8.2	7.2
Zn	61.5	51.3	8.1	53.8	36.3	41.0
Zr	37.1	33.1	261.9	36.4	42.2	42.1
Ag	< ld	< ld	< ld	< ld	< ld	< ld
Bi	5.1	5.2	6.0	4.6	5.1	5.2
Br	2.2	1.8	2.4	6.1	2.3	2.0
Cd	< ld	< ld	0.7	< ld	< ld	< ld
Cs	42.3	0.1	10.0	< ld	5.6	3.3
Ge	7	6.7	1.8	5.4	2.3	2.7
Hf	10.7	9.6	5.6	10.9	8.5	6.6
Hg	61.5	63.3	25.4	< ld	25.0	35.3
I	< ld	< ld	1.7	< ld	2.6	2.5
Mn	41.2	32.7	250.3	41.0	115.1	116.8
Sb	1.9	1.3	1.0	2.4	2.2	2.2
Se	0.2	0.1	0.1	< ld	0.3	< ld
Sm	< ld	2.5	0.4	< ld	1.4	0.9
Ta	2.5	1.9	3.8	9.5	3.5	3.2
Te	0.2	< ld	-0.3	0.5	2.0	< ld
Tl	3.7	2.1	2.5	1.2	1.1	1.2
U	4.3	4.2	6.8	2.7	7.7	6.0

Yb	7	3.2	5.0	5.6	5.6	4.2

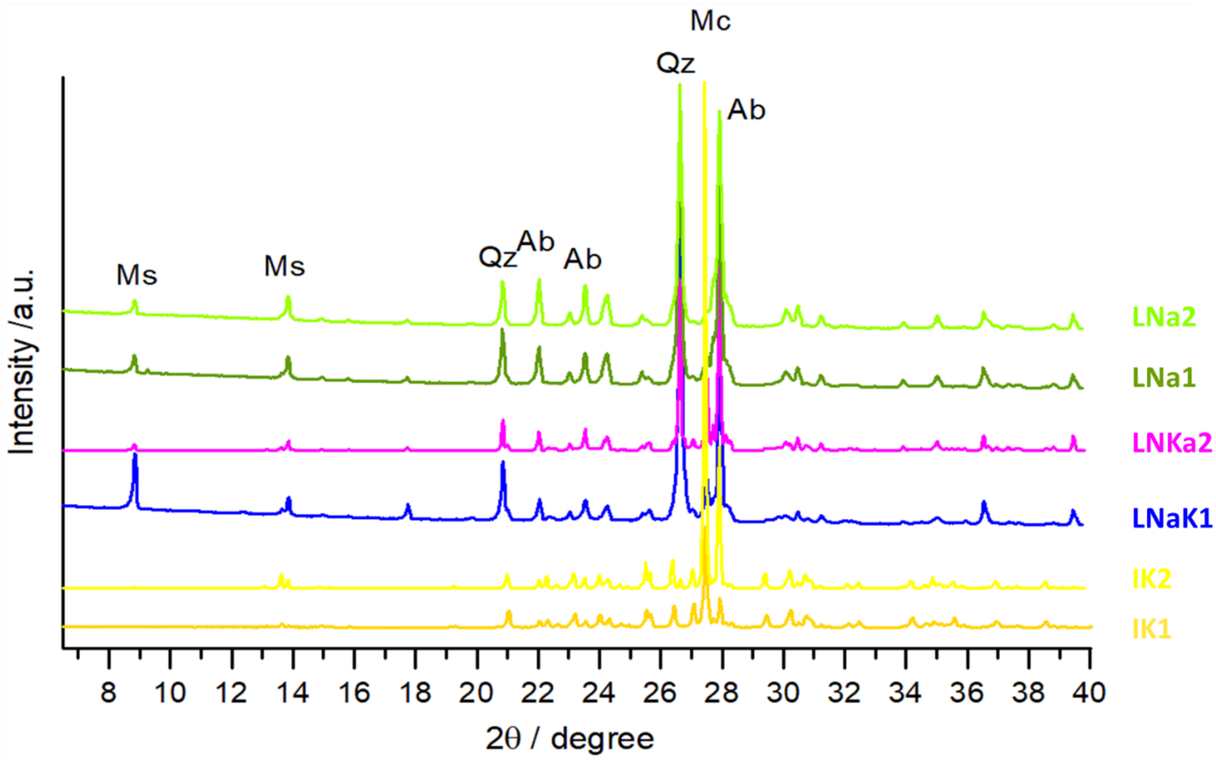

Figure S3. XRD spectra for all feldspar powders: LNa2, LNa1 (Na-rich); LNaK2, LNaK1 (K/Na); FK2, and FK1 (K-rich), collected over the 2θ range 8–40°. Identified phases include: mica (Ms), quartz (Qz), albite (Ab), and microcline (Mc).

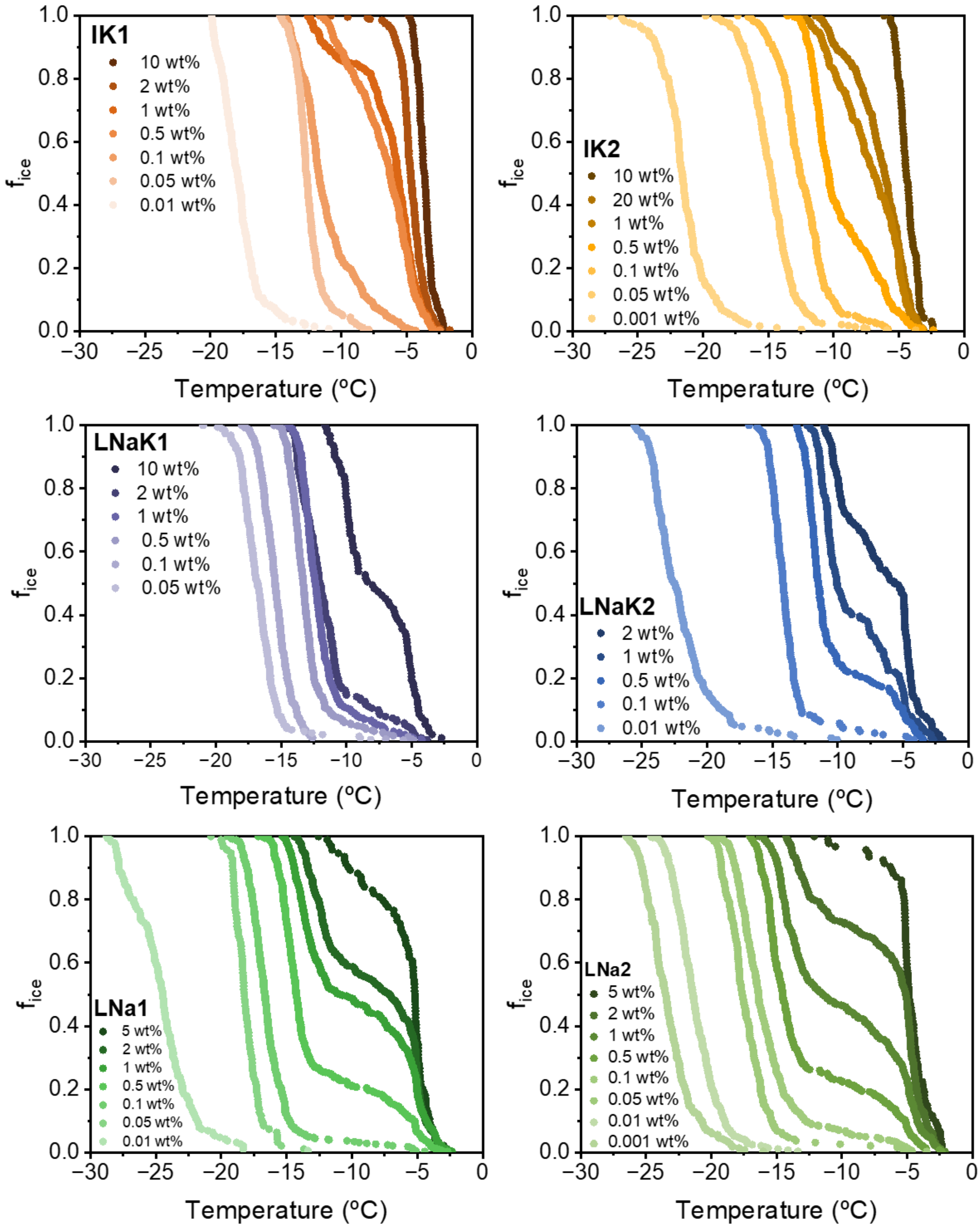

Figure S4. Fraction of frozen droplets, $f_{ice}(T)$ for all samples and concentrations tested. Top row: K-rich (IK1, and IK2). Middle row: K/Na similar ratio (LNaK1, and LNaK2). Bottom row: Na-rich feldspars (LNa1, and LNa2).

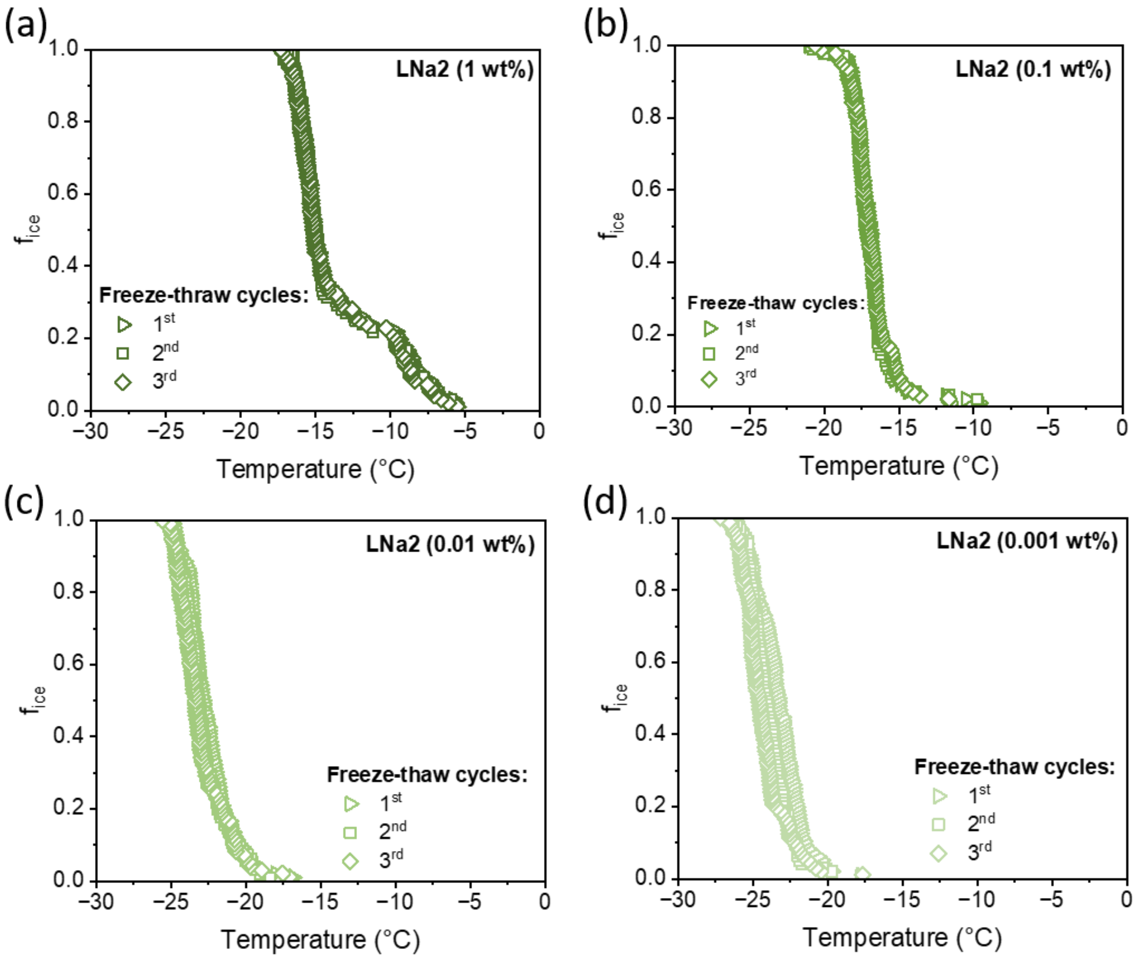

Figure S5. Freezing spectra of LNa2 feldspar suspensions at (a) 1 wt%, (b) 0.1 wt%, (c) 0.01 wt%, and (d) 0.001 wt%. The fraction of frozen droplets, $f_{ice}(T)$, is plotted for the first (△), second (□), and third (◇) freeze–thaw cycles. The overlap of successive cycles demonstrates the reproducibility of the freezing behavior.

Figure S6 shows the subpopulation analysis of LNa1 freezing spectra using HUB-backward *(de Almeida Ribeiro et al., 2023*) fits with three (a.1, a.2) and two (b.1, b.2) Gaussian components. Cumulative spectra, $N_m(T)$, (top) and corresponding differential spectra, $n_m(T)$, (bottom) demonstrate that the three-subpopulation model better reproduces the freezing onset and fitting shape, yielding an MSE of 0.0041 compared to 0.0652 for the two-subpopulation model. On the basis of this improved accuracy, the three-subpopulation fit was selected for subsequent analyses, with the corresponding parameters listed in Table S4.

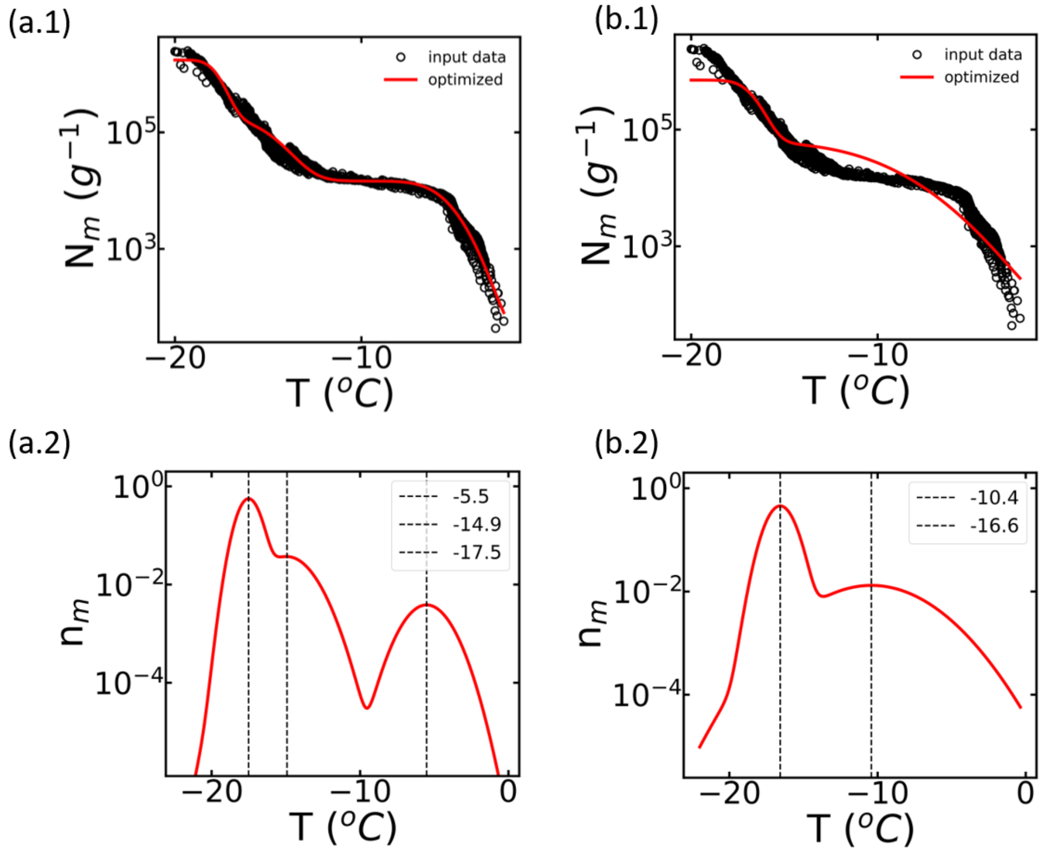

Figure S6. Subpopulation analysis of freezing experiments of the LNa1 feldspar powder suspension. Top panels: cumulative number of INs per unit mass, $N_m(T)$ (black circles) with HUB-backwards fits (red continuous lines) using (a.1) three, and (b.1) two subpopulations. Bottom panels: corresponding normalized differential spectra, $n_m(T)$; vertical dashed lines mark the mode temperatures (T_{mode}) of each subpopulation. Fit parameters are reported in Table S4.

Table S4. Parameters of the normalized distribution functions of the freezing spectra of LNa1 feldspar with three and two subpopulations. Temperatures of the corresponding subpopulation, and the probability of a droplet to freeze from each subpopulation. The mean squared error (MSE) describes the quality of the found optimized solution for the cumulative spectra obtained with the HUB analysis relative to the experimental cumulative spectra.

	Subpopulations	**SubP-A**		**SubP-B**		**SubP-C**		**MSE**
		T (ºC)	**%**	**T (ºC)**	**%**	**T (ºC)**	**%**	
LNa1	3	-5.51	1.16	-14.9	12.58	-17.51	86.26	0.0041
	2	-10.4	10.0	-16.57	90.0	-	-	0.0652

Table S3. Temperatures corresponding to the subpopulations of the differential freezing spectra shown in Figure 8 and the probability of a droplet to freeze from each subpopulation. * Probability has been calculated assuming that all droplets are frozen at -20 °C which is the case for densities below or approximately 0.01, see Figure 3.

	SubP-A		SubP-B		SubP-C		MSE
	T (ºC)	%*	T (ºC)	%	T (ºC)	%	
IK1	-5.4	0.3	-13.1	10.9	-17.4	88.7	0.0068
IK2	-6.1	0.8	-13.5	18.0	-16.4	81.2	0.0075
LNaK1	-5.7	0.2	-14.1	10.4	-16.5	89.4	0.0045
LNaK2	-5.6	0.4	-14.0	24.9	-16.0	74.61	0.0095
LNa1	-5.5	1.2	-15	12.6	-17.5	86.3	0.0041
LNa2	-5.5	0.8	-15.4	16.7	-18.0	82.4	0.0138

Table S5. Parameter of the normalized distribution functions of the freezing obtained through HUB method *(23)* using three Gaussian subpopulations of perthites published by *Whale et al. (2017)*: Orthoclase perthites (Dark Shap, Light Shap and LD4); Microcline perthites (KB14, Perthite, Keystone); and from *Harrison et al. (2016)*: nearly pure Albite and Microcline. Temperatures of the corresponding subpopulation, and the probability of a droplet to freeze from each subpopulation. The mean squared error (MSE) describes the quality of the found optimized solution for the cumulative spectra obtained with the HUB analysis relative to the experimental cumulative spectra.

	SubP-A		SubP-B		SubP-C		MSE
	T (ºC)	%*	T (ºC)	%	T (ºC)	%	
Dark Shap	-4	8.5	-11.9	20.2	-14.9	71.3	0.0035
Light Shap	-6.0	4.7	-13.9	19.4	-17.5	75.9	0.0063
LD4	-6.0	5.5	-14.5	25.8	-17.2	68.7	0.0085
KB14	-7.1	11.3	-12	41.3	-14.0	47.4	0.0033
Perthite	-6.1	5.5	-10.0	27.1	-13.0	67.5	0.0014
Keystone	-7.7	-0.1	-11.3	14.1	-14.1	86.0	0.0029

References

de Almeida Ribeiro, I., Meister, K., & Molinero, V. (2023). HUB: a method to model and extract the distribution of ice nucleation temperatures from drop-freezing experiments. *Atmospheric Chemistry and Physics*, *23*(10), 5623–5639. https://doi.org/10.5194/acp-23-5623-2023

Harrison, A. D., Whale, T. F., Carpenter, M. A., Holden, M. A., Neve, L., O'Sullivan, D., Vergara Temprado, J., & Murray, B. J. (2016). Not all feldspars are equal: A survey of ice nucleating properties across the feldspar group of minerals. In *Atmospheric Chemistry and Physics* (Vol. 16, Issue 17, pp. 10927–10940). Copernicus GmbH. https://doi.org/10.5194/acp-16-10927-2016

Whale, T. F., Holden, M. A., Kulak, A. N., Kim, Y. Y., Meldrum, F. C., Christenson, H. K., & Murray, B. J. (2017). The role of phase separation and related topography in the exceptional ice-nucleating ability of alkali feldspars. *Physical Chemistry Chemical Physics*, *19*(46), 31186–31193. https://doi.org/10.1039/c7cp04898j